Journal of Luminescence 194 (2018) 600–609

Contents lists available at ScienceDirect

Journal of Luminescence

journal homepage: www.elsevier.com/locate/jlumin

Synthesis, photophysical and electroluminescence studies of new triphenylamine-phenanthroimidazole based materials for organic light emitting diodes

Jairam Tagare[a], Hidayath Ulla[b], M.N. Satyanarayan[b], Sivakumar Vaidyanathan[a,*]

[a] Optoelectronic Laboratory, Department of Chemistry, National Institute of Technology Rourkela, India
[b] Department of Physics, National Institute of Technology Karnataka Surathkal, Mangalore, India

ARTICLE INFO

Keywords:
Green emitters
DFT
TPA derivatives
Undoped Organic light emitting diodes

ABSTRACT

In this work, two star-shaped small conjugated materials, namely tris(4-(1-phenyl-1H-phenanthro[9,10-d]imidazol-2-yl)phenyl) amine (PIPTPA) and tris(4-(1-p-tolyl-1H-phenanthro[9,10-d]imidazol-2-yl)phenyl)amine (PITTPA) with donor-π-acceptor (D-π-A) structures, were designed and synthesized by combining three phenanthroimidazole arms into an triphenylamine core. A detailed photophysical, thermal, electrochemical and related properties were systematically studied. Furthermore, theoretical calculations (DFT and TD-DFT) were performed to get a better understanding of the electronic structures. Both the materials were found to exhibit high glass transition temperatures (~ 238 °C) and high thermal stabilities with decomposition temperatures up to 298 °C. OLEDs using these materials as emissive materials showed excellent device performance (7.42 cd A^{-1}, 5.77 lm W^{-1}, 4.14% at 100 cd m^{-2}) with green emission and low turn-on voltages. The results demonstrate that TPA integrated with phenthroimdazole plays an important role in the device performance.

1. Introduction

An enormous research interest has developed in the field of organic light emitting diodes (OLEDs), because of their potential applications in the field of flat panel display and solid-state lighting [1–3]. OLEDs have several advantages like high brightness, fast response time, low driving voltage, self-emitting properties, full-color emission, with low cost and improved performances [4] For the commercial application of OLEDs, three basic color components (red, blue and green), are imperative for achieving energy efficient white light emission [5–7]. Spin-statistics suggest that the phosphorescent OLEDs (PhOLEDs) can achieve a maximum quantum efficiency (η_{int}) of 100% compared to that of fluorescent OLEDs (which can only reach up to η_{int} of 25%). However, PhOLEDs are limited with a shorter lifetime and a sharper efficiency roll-off at high brightness [8]. On the other hand, most of the reported high performances OLEDs contain dopant emitters in host materials, which usually require precise control of doping concentration and inevitably increase the manufacturing cost [9,10]. Also, it has been reported that a potential phase separation in the dopant-host system can render energy transfer an effective manner. For these reasons, undoped OLEDs using red, green and blue light-emitting fluorescent materials are still fascinating and getting considerable attention. Traditionally, the molecular structures of bipolar transport materials contain electron-donating (p-type) and electron-accepting (n-type) moieties [11]. One of the key factor for developing high-efficiency OLEDs is balanced charge injection and transport. The hole transport in many cases occurs through amine (e.g., diphenylamine, triphenylamine, carbazole) owing to their high hole mobility [12–14], whereas, electron-deficient heterocyclic moieties (e.g., triazines, oxadiazoles, pyridine, imidazole) can act as a good electron transporters [15–19]. Recent reports on non-doped OLEDs based on phenanthroimidazole derivatives have shown good efficiency and stability [20–22]. The stability of the compounds high due to the rigidity of the phenanthrene moieties [23]. The functionalization (both C_1 and N_1 position) of the phenanthroimidazole molecule with multiple moieties will lead to efficient device characteristics. Keeping this in view, we have designed and synthesized two star shaped green emitting materials containing a hole-transporting triphenylamine moiety and an electron-transporting phenanthroimidazole moiety with different substitution in the N_1-position (benzene and para-toluidine). The materials were characterized by spectroscopic methods and electrochemical analysis. The structures were optimized by using density functional theory (DFT) calculation and the locations of the energy levels (singlet and triplet) are calculated by using time-dependent DFT (TD-DFT) method. By integrating both

* Corresponding author.
E-mail address: vsiva@nitrkl.ac.in (S. Vaidyanathan).

http://dx.doi.org/10.1016/j.jlumin.2017.09.020
Received 13 March 2017; Received in revised form 5 September 2017; Accepted 8 September 2017
Available online 09 September 2017

theoretical data and experimental values we have calculated the energy gap (E_g) between the HOMO and LUMO levels. These star-shaped molecules show good thermal stability as well as a balanced charge transporting properties. Multilayer OLED devices have been fabricated using these molecules as emissive materials and the device has shown green color with appropriate CIE color coordinates.

2. Experimental section

2.1. General information for synthesis

All the reactions were performed under nitrogen atmosphere. Solvents were carefully dried and distilled from appropriate drying agents prior to use. Commercially available reagents (Sigma-Aldrich) were used without further purification unless otherwise stated. All the reactions were monitored by thin-layer chromatography (TLC) with silica gel 60 F_{254} Aluminum plates (Merck). Column chromatography was carried out using silica gel (Sigma-Aldrich).

2.2. Measurements

^{1}H NMR and ^{13}C NMR spectra were recorded using an AV 400 Avance-III 400 MHz FT NMR Spectrometer (Bruker Biospin International, Switzerland) with tetramethylsilane (TMS) as a standard reference. The FTIR spectra were recorded on a Perkin–Elmer RX-I FTIR spectrophotometer. Elemental analysis was obtained using Elementary Analysis Systeme, Germany/Vario EL spectrometer. The mass spectra were recorded by LC–MS (Perkin–Elmer, USA/Flexer SQ 300M). Powder XRD data of the materials were recorded with Cu-Kα1 radiation (Rigaku, ULTIMA IV). DSC-TGA was performed using Netzshe, Germany, STA449C/4/MFC/G. The absorption spectrum of the target compound in solution phase and solid (DRS) were measured by using UV–visible spectrometer (Shimadzu Corporation, Japan/UV-2450 Perkin Elmer, USA/Lamda 25). The optimized structures and HOMO-LUMO energy levels were calculated by using DFT calculation with B3LYP/6-31G (d,p) basis set. All calculations were carried out using Gaussian09 W 29 and GaussianView suite of programs. The photoluminescence emission spectra were recorded by Horiba Jobin Yvon, USA/Fluoromax 4P spectrophotometer. The lifetime of the materials was measured at 298 K with Edinburgh Instruments FLS 980 and a pulsed xenon lamp was used as the excitation source. The electrochemical properties of the target materials were performed by Cyclic Voltammetry (CV) in dichloromethane. For solution process, CV analysis was done by using working, auxiliary (counter) and reference electrodes. The corresponding electrodes are glass-carbon disk, Pt wire, and Ag/AgCl wire respectively. The dichloromethane which contains 0.1 M Bu_4NClO_4 was used as reference electrolyte.

2.3. Synthesis procedure

2.3.1. Tris(4-formyl phenyl) amine (TPA-CHO)

Triphenylamine (4.9 g, 20 mmol) and anhydrous DMF (40 mL) were added to a 250 mL two neck round bottom flask under nitrogen. The mixture was cooled to 0 °C and phosphorus oxychloride (37.0 mL, 420 mmol) was added dropwise via syringe. The progress of the reaction was monitored by TLC (EtOAC in hexanes 2:8, Rf-0.6). The resulting mixture was stirred for 2 days at 95 °C. Further it was poured into water and neutralized with diluted sodium hydroxide solution. Then, it was extracted with dichloromethane. This was followed by drying over sodium sulfate and the solvent was removed to get 3.5 g of crude TPA-CHO. The crude product was purified by column chromatography by using silica gel (100–200 mesh) and eluent ethyl acetate in hexanes (2:8) to obtain pure product (2.45 g, yield 37.2%) with pale yellow colored fine solid. ^{1}H NMR (400 MHz, $CDCl_3$, TMS, δ ppm) 9.96 (s, 3H), 7.87–7.85 (d, 6H), 7.27–7.25 (d, 6H), ^{13}C NMR (100 MHz, $CDCl_3$, TMS, δ ppm) 190.47, 151.20, 132.60, 131.50, and 124.53.

2.4. General procedure for the synthesis of the triphenylamine-phenanthreneimidazole derivatives

Amine (0.87 g, 9.39 mmol) was added to a stirred solution of TPA-CHO (1 g, 3.03 mmol) in glacial acetic acid (60 mL) at room temperature (RT). To this reaction mixture, subsequently ammonium acetate (9.3 g, 121.2 mmol) and 9, 10-phenanthrenequinone (1.95 g, 9.39 mmol) were added. The resulting mixture was stirred for 12 h at 125 °C. The reaction was monitored by thin layer chromatography for the completion of the reaction. After cooling, the reaction mass was poured into ice cold water then neutralized with ammonium hydroxide solution. The reaction mass was concentrated with dichloromethane. This was followed by drying with anhydrous sodium sulfate and the solvent was evaporated to get crude phosphor. The resultant phosphor was purified with column chromatography by using silica gel (100–200 mesh) and eluent methanol in dichloromethane (1:9). The solvent was then evaporated and the residue was dissolved in minimum amount of THF solution. To this solution, excess of hexane solvent was added to form a fine precipitate. After the precipitate had completely settled down, the solvent was decanted.

tris(4-(1-phenyl-1H-phenanthro [9,10-d] imidazol-2-yl)phenyl) amine (PIPTPA): Yield: 65%. ^{1}H NMR (400 MHz, $CDCl_3$, TMS, δ ppm) 8.89 (d, J = 7.6 Hz, 3H), 8.79 (d, J = 8 Hz, 3H), 8.73 (d, J = 8.4 Hz, 3H). 7.78 (t, J = 7.2 Hz, 3H), 7.75-7.67 (m, 12H), 7.65 (m, 6H), 7.59 (d, J = 1.6 Hz, 6H), 7.51 (m, 6H), 7.19 (d, J = 7.6 Hz, 3 H), 6.97 (d, J = 8.8 Hz, 6H). ^{13}C NMR (100 MHz, $CDCl_3$, TMS, δ ppm) 149.94, 149.53, 146.65, 138.34, 136.92, 129.98, 129.75, 129.72, 129.50, 128.71, 128.64, 127.77, 127.64, 126.75, 125.78, 125.09, 124.32, 123.61, 123.29, 122.62, 122.54, 122.25, 120.31, IR (KBr, ν/cm^{-1}): 3430, 3058, 1665, 1599, 1469, 1322, 1263, 1103, 813, 757. EI-MS: m/z = 1123.01 [M + H] $^+$. CHNS Analysis: Anal. Calc. for $C_{81}H_{51}N_7$: C, 86.68; H, 4.58; N, 8.74; Found: C, 86.87; H, 4.92; N, 9.21%.

tris(4-(1-p-tolyl-1H-phenanthro [9,10-d] imidazol-2-yl)phenyl) amine (PITTPA): Yield: 71%. ^{1}H NMR (400 MHz, $CDCl_3$, TMS, δ ppm) 8.88 (d, J = 1.2 Hz, 3H), 8.78 (d, J = 8.4 Hz, 3H), 8.72 (d, J = 8.4 Hz, 3H). 7.75 (t, J = 7.2 Hz, 3H), 7.66 (t, J = 1.2 Hz, 3H), 7.58-7.50 (m, 9H), 7.45-7.43 (m, 12H), 7.32-7.003 (m, 6H), 6.98 (d, J = 5.4 Hz, 6H), 2.60 (s, 9H). ^{13}C NMR (100 MHz, $CDCl_3$, TMS, δ ppm) 149.94, 146.63, 139.62, 136.83, 135.64, 130.41, 130.34, 129.73, 129.61, 128.68, 128.25, 127.75, 126.68, 125.74, 125.00, 124.89, 124.24, 123.54, 123.33, 123.21, 122.64, 122.60, 122.22, 21.10. IR (KBr, ν/cm^{-1}): 3440, 3056, 1669, 1599, 1469, 1322, 1291, 1183, 1108, 836, 756. EI-MS: m/z = 1164. 85 [M + H] $^+$. CHNS Analysis: Anal. Calc. for $C_{84}H_{57}N_7$: C, 86.65; H, 4.93; N, 8.42. Found: C, 86.89; H, 5.15; N, 8.75%.

2.5. OLED fabrication and measurements

For OLED fabrication, pre-patterned ITO (Kintec) coated glass substrates with a sheet resistance of 15 Ω/□ and ITO thickness of 120 nm were used as anodes. The pre-cleaning and UV-Ozone treatment of ITO–glass substrates were carried out according to the reported earlier. All the organic materials and the cathode layers were thermally evaporated at a base pressure of 5×10^{-6} Torr. On the ITO substrate, the HIL, HTL, emitting layer, HBL, EIL, and cathode were deposited. F_4TCNQ (LUMTEC) was used as HIL, α-NPD (LUMTEC) was used as the HTL, BCP (Sigma-Aldrich) was used as HBL, LiF (Sigma-Aldrich) was used as EIL and Al (Alfa Aesar) was used as the cathode. The deposition rate of organic materials was maintained at 0.5 Å s^{-1}, whereas the deposition rates of LiF and Al were 0.1 Å s^{-1} and 6 Å s^{-1} respectively. The deposition rate and thickness of the deposited layers were controlled in situ by a quartz crystal thickness oscillator placed near the substrate. The cathode was deposited on the top of the structure through a shadow mask to form active emission area of 1.6 mm^2. All the organic and cathode layers were deposited simultaneously and the devices were never exposed to air during fabrication. All the properties of OLEDs such as EL spectra, J-V-L characteristics of the devices were

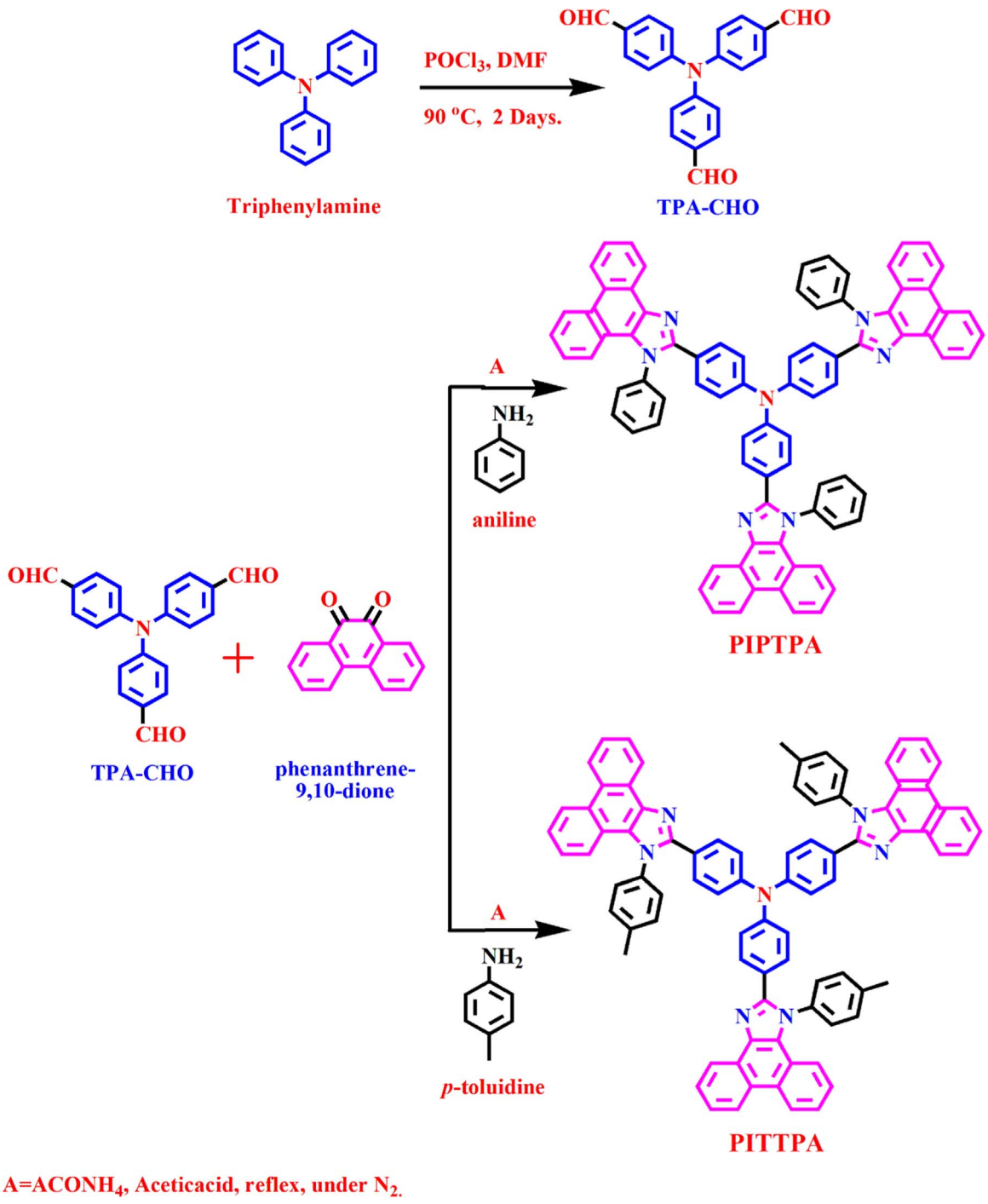

Scheme 1. Synthetic routes for the triphenylamine-phenanthreneimidazole derivatives.

measured using a spectrophotometer (Horiba Jobin Yvon iHR320), a computer-controlled, programmable source-meter (Keithley 2400) and Si photodiode (SM1PD2A). CIE coordinates were calculated from the EL spectra. All the measurements were carried out at room temperature under ambient conditions without any encapsulation and the devices were driven under dc conditions

3. Results and discussion

3.1. Synthesis

Synthesis of triphenylamine-phenanthreneimidazole derivatives were accomplished as illustrated in Scheme 1. The tris(4-formyl phenyl) amine (TPA-CHO) intermediates were synthesized according to the literature with modified procedures [24]. The targated PIPTPA and PITTPA materials were synthesized by condensation between 9, 10-phenanthrenequinone, substituted amine and TPA-CHO in the presence of ammonium acetate and acetic acid. The structures of products were confirmed by NMR, mass spectrometry and IR spectroscopy.

3.2. Fourier transform infrared (FT-IR) spectroscopy

The FTIR spectrum of the PIPTPA and PITTPA materials were measured in the wavenumber range 500–4000 cm^{-1} (Fig. 1) and the wavenumbers are displayed in Table 1. The peak at approximately 3440 cm^{-1} corresponds to ≥ C–H in both the materials.[25]

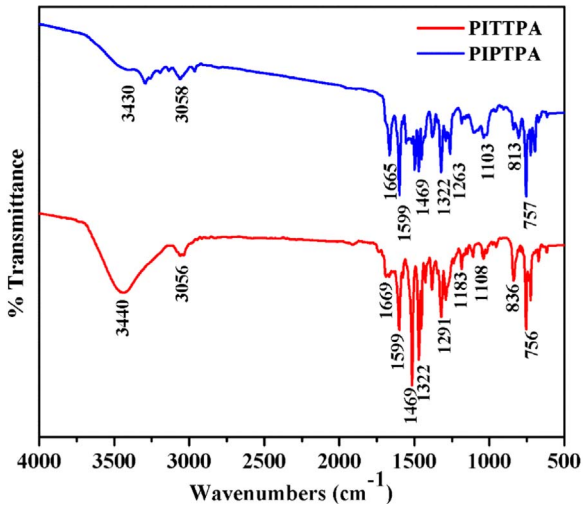

Fig. 1. FTIR spectra of the PIPTPA and PITTPA materials.

Table 1
IR data of PIPTPA and PITTPA materials.

Bonding	PIPTPA	PITTPA
C = N	1665	1669
NH–CH	3430, 3058	3440, 3056
Aromatic C–C, C = C stretching frequency.	1599, 1469, 1322, 1263	1599, 1469, 1322, 1291,1183
C–H bending	1003, 813, 757	1108, 836, 756

(Generally, the IR spectrum of the nitrogen-containing heterocyclic compounds show absorption peak at ~ 3400 cm^{-1}). The frequency around 1650 cm^{-1} corresponds to the C=N function of imidazole and frequency around 1599 cm^{-1} corresponds to C=C aromatic segments. The peak at ~750 cm^{-1} is likely due to the aromatic C–H bending.

3.3. Powder XRD studies

Powder XRD studies were performed to evaluate the crystalline or amorphous nature of the synthesized materials are shown in Fig. 2. XRD pattern of the materials were recorded in the 2θ range between 10° and 60°. The diffraction peaks of both the materials show amorphous phase without the appearance of any peak. In general, amorphous materials are highly required to fabricate the OLEDs, where the materials should not be crystalline in the device operating conditions. The currently synthesized materials are potential to be used as emissive materials in the OLED device.

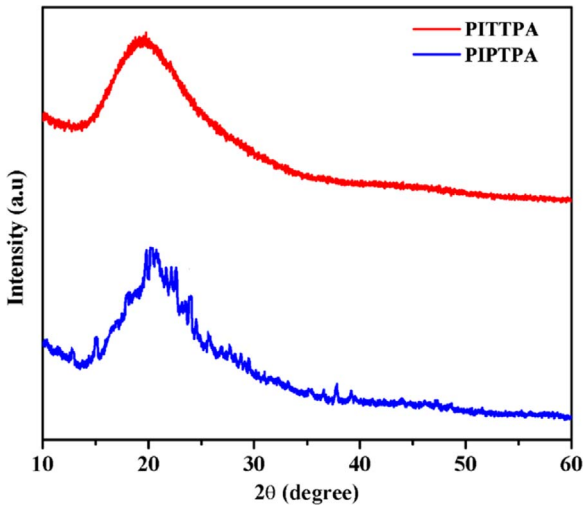

Fig. 2. Powder X-ray diffraction patterns of PIPTPA and PITTPA materials.

3.4. Thermal properties

The durability and lifetime of the device are correlated with the glass transition temperature (T_g) [26]. The thermal behavior of PIPTPA and PITTPA were investigated by differential scanning calorimetry (DSC) and thermogravimetric analysis (TGA) under a nitrogen atmosphere. DSC-TGA measurements were carried out from 0° to 700 °C at a scanning rate of 10 °C/min. DSC-TGA curves of synthesized materials were depicted in Fig. 3. The TGA curves reveal that the decomposition temperature (T_d) of 10% weight loss of PIPTPA and PITTPA is 269 °C and 298 °C, respectively. In addition, these materials exhibit high glass transition temperature (T_g = 233 °C, PIPTPA and 238 °C, PITTPA), which is distinctly higher than that of reported related fluorophores [27]. The significant enhancement of T_g can be attributed to the addition of two phenanthroimidazole moieties, which are likely to improve their morphological stability greatly. These DSC-TGA results suggest that the currently investigated materials possess high thermal decomposition temperature which is one of the essential requirements for OLEDs.

3.5. Photophysical properties

The optical properties of the two materials were evaluated by measuring UV–Vis absorption and photoluminescence (PL) spectra in both chloroform solution (Fig. 4A) as well as in solid-state thin film form on quartz substrates (Fig. 4B). The obtained key photophysical data is summarized in Table 2. The absorption band occurred at a wavelength of approximately 260 nm is attributed to the π–π* transition of benzene ring [28]. The longer wavelength absorption band occurred at a wavelength of approximately 375 nm might have originated from the π–π* transition of TPA and phenanthroimidazole moieties. The optical bandgap of the materials (PIPTPA and PITTPA) was calculated from the diffuse reflectance spectra (DRS) with the help of Kubelka-Munk function (Fig. S9 in Supplementary information) [29]. The former shows optical band gap of 2.62 eV, whereas the latter shows 2.71 eV (Table 3). Both the materials show blue emission with emission maxima at 429 (PIPTPA) and 427 nm (PITTPA) in solution. However, in thin film form, both the absorption, as well as emission bands, are red shifted (Table 2). Similar observations were observed for solid PL spectra (Fig. 4B). The observed redshifts can be explained by their relative strong π–π stacking interactions [30]. The CIE chromaticity coordinates for materials is shown Fig. 4C. It is very clear from the picture that the color changes from blue to green, by simply going from solution to solid through a thin film (confirmed from Fig. 4A and B).

Fluorescence quantum yield (Φ_f) is an important parameter for the quantitative characterization of materials. The Φ_f of the materials were calculated by using 9, 10- diphenyl anthracene as a standard (Φ_{ref} = 0.90 in cyclohexane) according to the Eq. (1) [31],

$$\Phi_f = \Phi_{ref}\left(\frac{S_{sample}}{S_{ref}}\right)\left(\frac{A_{ref}}{A_{sample}}\right)\left(\frac{n^2_{sample}}{n^2_{ref}}\right) \quad (1)$$

where S_{sample}, A_{sample}, n_{sample} and S_{ref}, A_{ref}, n_{ref} represent the integrated emission band area, the absorbance at the excited wavelength, and the refractive index of the solvent, respectively for the standard reference and the sample. The quantum yields of the materials are 0.25 (PIPTPA) and 0.27 (PITTPA), respectively.

The fluorescence lifetime of the PIPTPA and PITTPA materials at 10^{-5} M concentrations were measured using time-correlated single photon counting technique and the decay curves are shown in Fig. 4D. The decays were fitted mono-exponential function given by the equation (t) = I_0 + A_1 exp(-t/τ), where I_0 = 0 is the offset value, A_1 is the

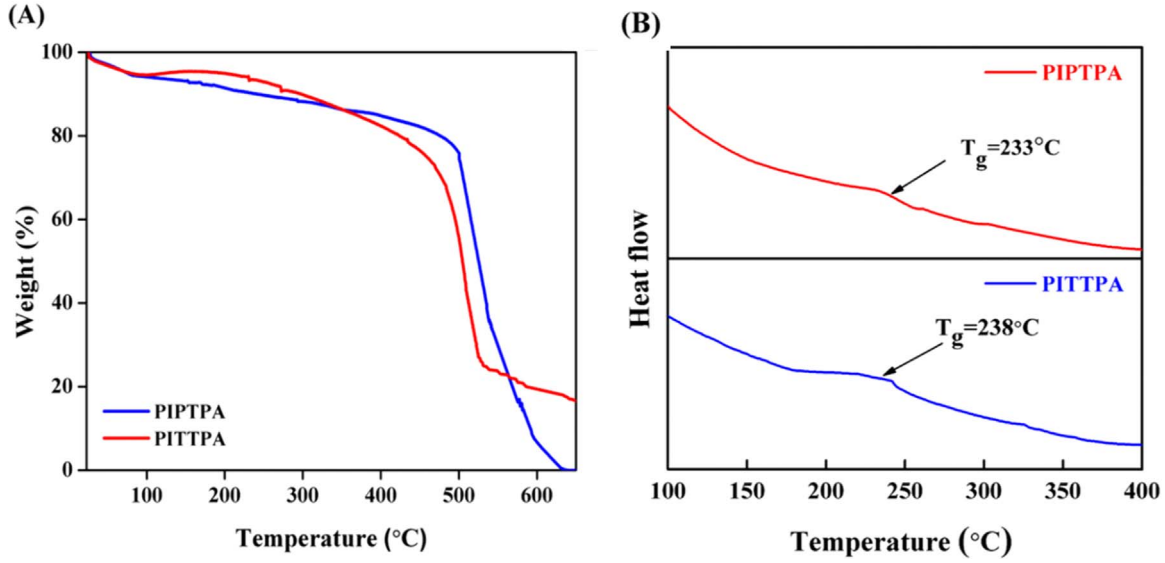

Fig. 3. (A) TGA and (B) DSC curves of PIPTPA and PITTPA at a heating rate of 10 °C/min.

scalar quantity obtained from the curve fitting, t is the time in μs and τ is the decay time value for the exponential component. The fluorescence lifetime of PIPTPA and PITTPA materials were found to be 2.07 and 1.97 μs (Table 2).

3.6. Solvatochromism study

Solvatochromism study was also been carried out for PIPTPA and PITTPA. Interaction of solvent-dependent emission spectra appears to

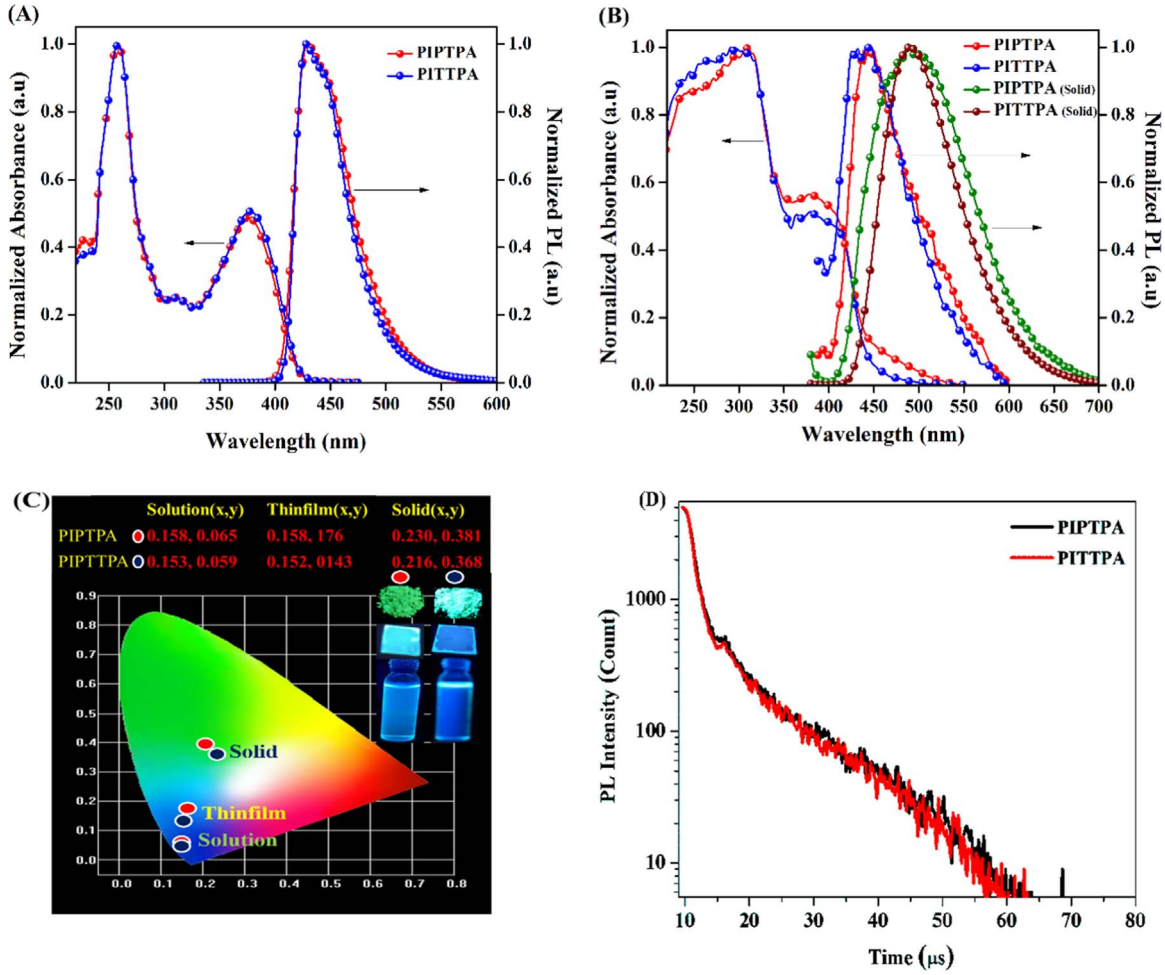

Fig. 4. (A) UV absorption and PL spectra of PIPTPA and PIPTTPA in $CHCl_3$ solution, (B) in the film and solid state, (C) the CIE chromaticity coordinates for materials (D) Fluorescence lifetime decay curves.

Table 2
Key photophysical properties of PIPTPA and PITTPA materials.

Compounds	T_g[a]/T_d[a] °C	Solution		Φ_f[b]	Life time (τ_1) in μs	Film		Solid PL (nm)
		Abs (nm)	PL (nm)			Abs (nm)	PL (nm)	
PIPTPA	233/475	258, 375	429	0.25	2.07	308, 383	446	495
PITTPA	238/495	256, 377	427	0.27	1.97	306, 387	440	487

[a] Glass transition temperature, thermal decomposition temperature.
[b] Fluorescent quantum yield in solution measured with respect to diphenyl anthracene.

be simple but it is complicating due to the molecules multiple interactions with their local environment, which results in spectral (either blue or red) shifts. The emission of the materials was accomplished under different solvents: toluene, tetrahydrofuran (THF), chloroform ($CHCl_3$), dichloromethane (DCM), dimethylformamide (DMF), and acetonitrile (ACN) and their Stoke's shifts were calculated. The solvatochromism of materials was interpreted in terms of Lippert-mataga equation. It defines the Stokes shift in terms of the changes that occur in the dipole moment during excitation. By increasing the polarity of the solvent, the red (bathochromic) shift was observed, which are showed in Fig. 5 (PIPTPA) and Fig. 6 (PITTPA). The Eqs. (2) and (3) of Lippert–Mataga describes the solvatochromic Stokes shift $\Delta\bar{\nu}$ (expressed in wavenumbers) as a function of the change of the dipole moment $\Delta\mu_{ge} = \mu_e - \mu_g$ of the phosphors. Solvents with dissimilar dielectric constants (ε) and refractive indices (n) are used in the Eq. (3) and the plot was drawn Stokes shift ($\Delta\bar{\nu}$) as a function of Δf [32].

$$\Delta\bar{\nu} = \frac{2\Delta f}{4\pi\varepsilon_0 hca^3}(\mu_e - \mu_g) + \text{ Constant} \quad (2)$$

$$f(\epsilon) = \frac{f(\epsilon-1)}{f(2\epsilon+1)} \text{ And } f(n^2) = \frac{(n^2-1)}{(2n^2+1)} \quad (3)$$

where $\Delta\bar{\nu} = \Delta\bar{\nu}_{abs} - \Delta\bar{\nu}_{em}$ is the solvatochromic shift (in cm^{-1}) between the maxima of absorption and fluorescence emission [$\Delta\bar{\nu}_{abs} = 1/\lambda_{abs}$ (max), $\Delta\bar{\nu}_{em} = 1/\lambda_{em}$ (max)], h is Planck's constant, c is the velocity of light, ε_0 is the permittivity of vacuum (signifies the radius of the cavity in which the solute resides); μ_e and μ_g are dipole moments in the excited and ground states. The solvatochromism data is tabulated in Table S1 (Supplementary information). It was also verified using Lippert–Mataga equation (Fig. S10 in Supplementary information). Fig. S10 represents the Lippert–Mataga plot for PIPTPA and PITTPA in different solvents. Fig. S10 (A) indicates the linear relationship [correlation coefficient r = 0.515, slope = (4.423) × 10^3 cm^{-1}, intercept = (6.717) × 10^3 cm^{-1}] of the Stokes shift, $\Delta\bar{\nu}$ verses Δf for different solvents of PIPTPA. Similarly, Fig. S10 (B) indicates the linear relationship [correlation coefficient r = 0.514, slope = (2.351) × 10^3 cm^{-1}, intercept = (6.974) × 10^3 cm^{-1}] of the Stokes shift, $\Delta\bar{\nu}$ verses Δf for PITTPA.

3.7. Theoretical calculations

To gain insight into the electronic structures of the materials, density functional theory (DFT) calculation was performed at the B3LYP/6-31G (d,p) basis set [33]. The DFT-calculated optimized geometries of these materials (Fig. 7) in gas phase show slightly twisted conformations. In PITTPA, dihedral angles between Phenanthroimidazole and triphenylamine plane (28.4°) is slightly more than PIPTPA (24.66°), due to a twisted substituent on the 1-imidazole position. As shown in Fig. 7, the HOMO levels mainly populate on the triphenylamine (TPA) for both the phosphors, whereas, the *LUMO* were exclusively located on phenanthroimidazole moiety. The calculated HOMO/LUMO values of the materials are − 4.71/− 1.19 eV (PIPTPA) and − 4.73/− 1.23 eV (PITTPA), respectively. The expected HOMO–LUMO energy gaps of 3.50 (PIPTPA) and 3.52 eV (PITTPA) are well in alignment with the experimental results (Table 3). The singlet and triplet energy levels are calculated by using time-dependent density functional theory (TD-DFT) analysis and are included in Table 3. In addition, atom coordinates and absolute energies of PIPTPA and PITTPA were given in Supplementary information (SI3 in Supplementary information).

3.8. Electrochemical properties

The electrochemical properties of both the materials were investigated by cyclic voltammetry (CV) using 0.1 M tetrabutylammonium perchlorate (Bu_4NClO_4) as a supporting electrolyte in anhydrous dichloromethane (DCM) solution at a scan rate of 100 mV s^{-1}. The cyclic voltammograms are shown in Fig. 8 and the corresponding electrochemical data is summarized in Table 3. Fig. 8 shows that both the materials have distinct oxidation and reduction behaviors, which clearly indicate their potential bipolar carrier transporting nature. According to the onset potentials, we calculated the highest occupied molecular orbital (HOMO) and the lowest unoccupied molecular orbital (LUMO) energy levels by using the Eqs. (4) and (5) reported by de Leeuw et al. [34].

$$E_{HOMO} = -(E_{ox}^{onset} + 4.4)\text{ eV} \quad (4)$$

$$E_{LUMO} = -(E_{red}^{onset} + 4.4)\text{ eV} \quad (5)$$

The HOMO/LUMO energy levels of the molecules are − 5.38/− 3.12 eV (PIPTPA) and − 5.71/− 2.97 eV (PITTPA), respectively with energy bandgap of 2.71 (PIPTPA) and 2.74 eV (PITTPA). The HOMO-LUMO results of both the materials suggest that they can be used as host materials as their HOMO/LUMO energy levels are similar to

Table 3
Electrochemical properties of PIPTPA and PITTPA materials.

Compounds	E_{ox}[a] (V)	E_{red}[a] (V)	HOMO (eV)	LUMO (eV)	E_g[b] (eV)	E_g[c] (eV)	E_g[d] (eV)	S_1[e] (gas) (eV)	T_1[f] (gas) (eV)
PIPTPA	1.43	− 1.28	− 5.83	− 3.12	2.62	2.71	3.50	3.060	2.49
PITTPA	1.31	− 1.43	− 5.71	− 2.97	2.71	2.74	3.52	3.068	2.50

[a] The onset potential.
[b] Optical energy bandgap estimated from the solid-state absorption spectra.
[c] Electrochemical bandgap determined from cyclic voltammetry.
[d] Theoretical bandgap.
[e] Singlet energy.
[f] Triplet energy.

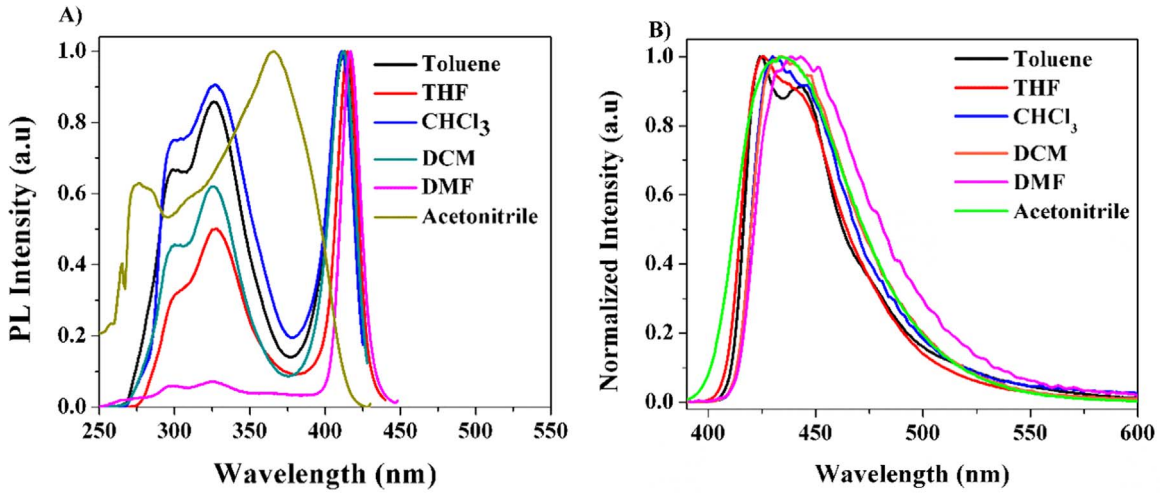

Fig. 5. (A) Excitation and (B) emission spectra of PIPTPA in different solvents.

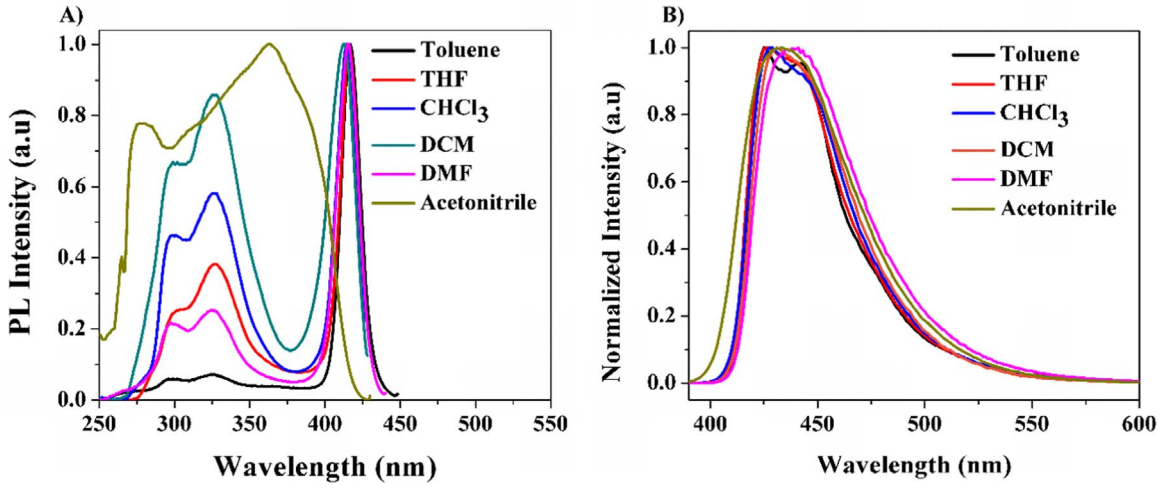

Fig. 6. (A) Excitation and (B) emission spectra of PITTPA in different solvents.

commercially available host materials like CBP [35]. The comparison of HOMO-LUMO energy gap of both the molecules is shown in Fig. 9. It clearly indicates that the band gaps calculated using both optical and electrochemical analyses almost match.

3.9. Electroluminescence studies

To investigate the electroluminescent properties of TPA derivatives (PIPTPA and PITTPA) as emissive materials, OLEDs were fabricated with the device configuration: ITO (120 nm)/F_4TCNQ (4 nm)/α-NPD (40 nm)/TPA derivatives (50 nm)/BCP (10 nm)/LiF (0.5 nm)/Al (150 nm). The related HOMO/LUMO energy levels of the derivatives along with other materials used in the electroluminescent devices are illustrated in Fig. 10. Here ITO (indium-tin oxide) served as a transparent anode, F_4TCNQ (2,3,5,6-Tetrafluoro-7,7,8,8-tetracyano quinodimethane) as hole-injection layer (HIL), α-NPD (4,4'-bis[N-(1-naphthyl)-N-phenyl-l-amino]-biphenyl) as the hole-transporting layer (HTL) and BCP (bathocuproine) as hole-blocking layer (HBL); LiF (lithium fluoride) and Al (aluminum) were used as the electron-injecting layer (EIL) and cathode, respectively. F_4TCNQ was chosen as HIL as it efficiently injects holes from the ITO anode to hole-transport-layer α-NPD. An optimized thickness of F_4TCNQ was used for better hole injection as reported earlier [36,37]. By using BCP as HBL, the reductant holes are confined in the emitting layer which didn't recombine with the electrons in the emitting zone [38,39]. The current density-voltage-luminance (J-V-L) characteristics of the fabricated OLEDs are shown in Fig. 11 A. The characteristics of the current density as a function of applied voltage reveal good diode behavior. The devices utilizing PIPTPA and PITTPA exhibit drive voltage (corresponding to 1 cd/m^2) of 3.08 and 2.95 V, respectively. Both the devices exhibited good current density demonstrating good charge transport capability. The devices showed maximum luminance (L_{max}) of 11711 cd/m^2 (PIPTPA) and 10,844 cd/m^2 (PITTPA) at 15 V. The current, output power and external quantum efficiencies for both the devices along with other parameters of the devices are summarized in Table 4. Out of the two derivatives investigated, a device fabricated with PIPTPA as emissive materials showed current efficiency (η_c) of 7.42 cd/A, power efficiency (η_p) of 5.77 lm/W and external quantum efficiency (η_{ext}) of 4.14% corresponding to 100 cd/m^2. The results suggest that though the derivatives have comparatively moderate EL quantum efficiency, the charge carrier balance is significantly strong (injection barrier for holes and electrons) which results in high EQE (EQE = $\gamma\,\chi\,\eta_{pl}\,\eta_{oc}$, where γ is the recombination efficiency of injected holes and electrons, χ is the fraction of excitons that can potentially radiatively decay due to restriction of multiplicity, η_{PL} is the PL yield and η_{oc} is the out-coupling efficiency) [40]. This may arise from the relatively low barrier for the hole and electron injection from the HTL and ETL, respectively into the active layers. Fig. 11 B depicts the steady-state electroluminescence (EL) spectra of the devices at the driving voltages of 10 V with PIPTPA and PITTPA as emitter molecules with green light emission with peaks

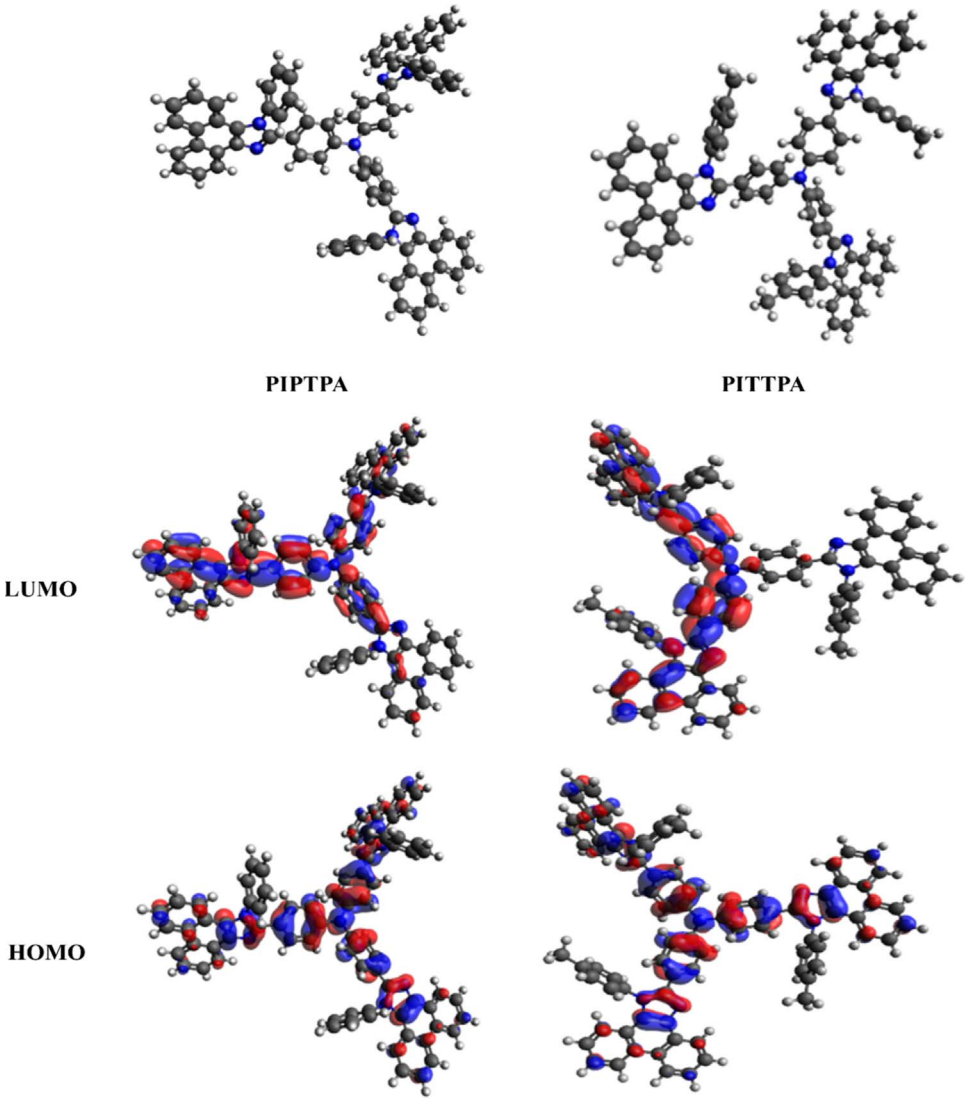

Fig. 7. Spatial distributions of frontier orbitals of PIPTPA and PITTPA materials.

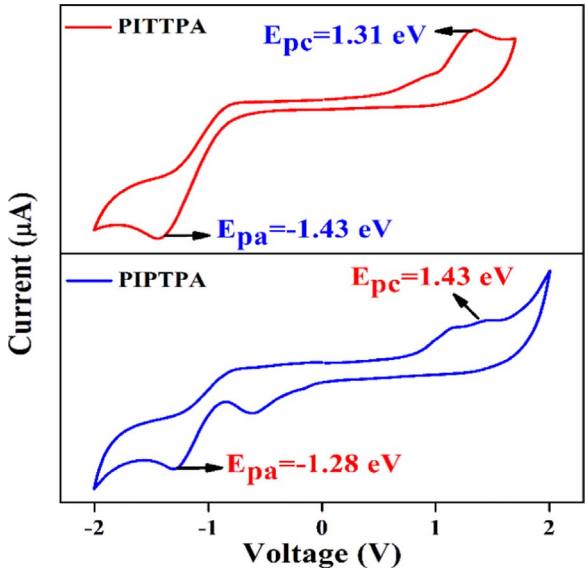

Fig. 8. Cyclic voltammogram of PIPTPA and PITTPA materials.

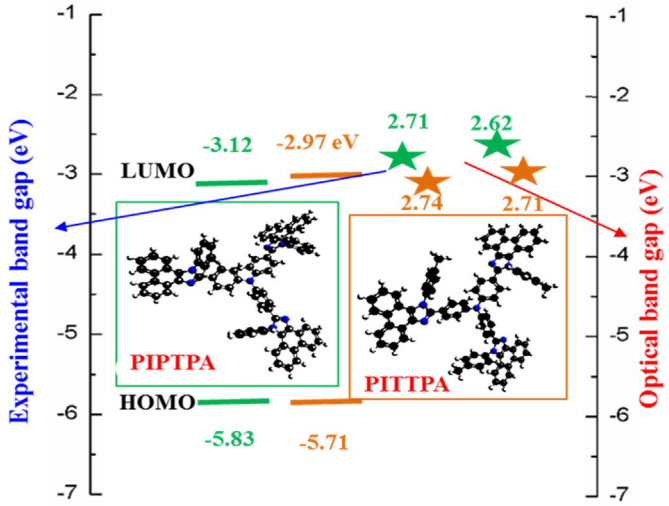

Fig. 9. HOMO–LUMO energy gap diagram of PIPTPA and PITTPA materials.

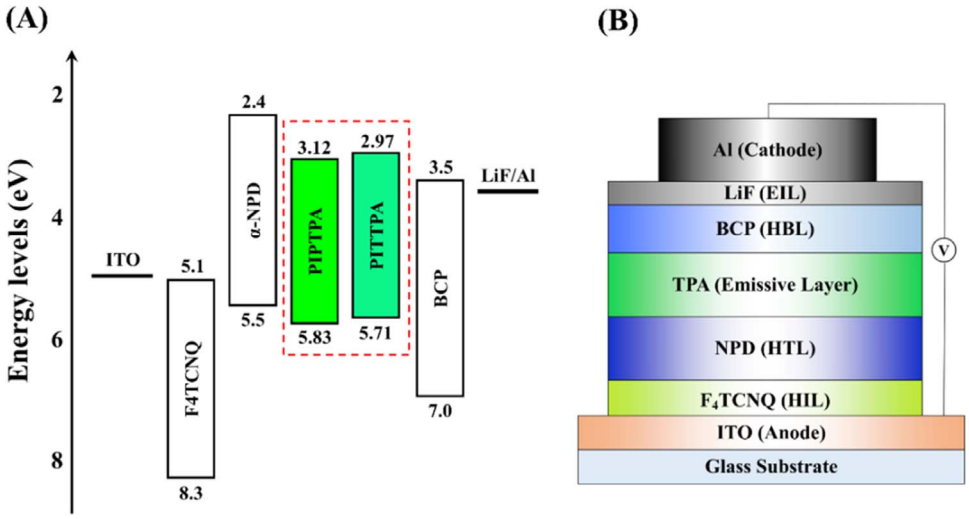

Fig. 10. (A) Energy-level diagram of the materials and (B) Schematic diagram of the OLED structure used in this study.

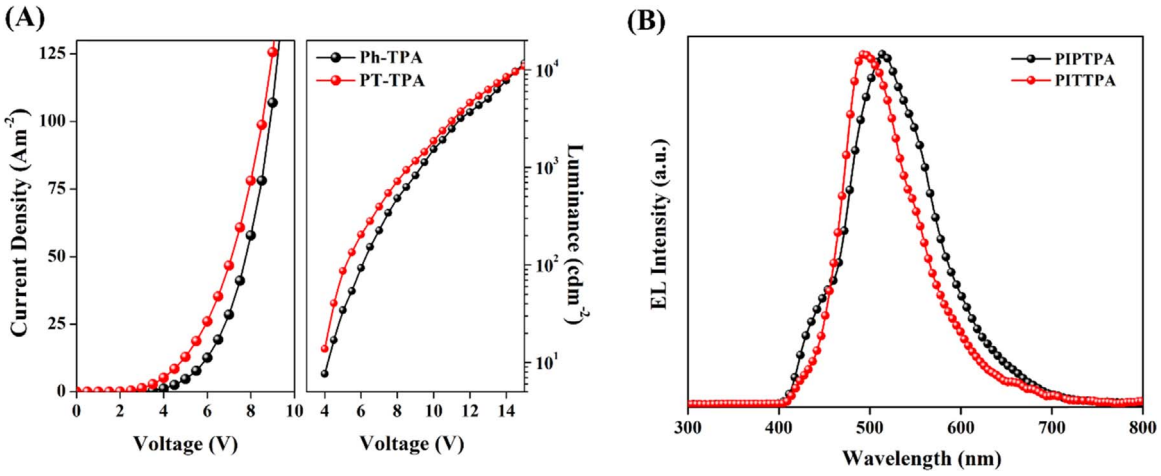

Fig. 11. (A) Current density–voltage–luminance (J–V–L) characteristics, and (B) EL spectra of the OLEDs with TPA as emissive materials.

Table 4
Electroluminescent performance data of OLEDs using TPA derivatives as emissive materials.

Device[a]	V_{onset} (V)[b]	L_{max} (cd m^{-2})[c]	η_c (cd A^{-1})[d]	η_p (lm W^{-1})[d]	η_{ext} (%)[d]	λ_{em} (FWHM) (nm)[e]	CIE$_{(x,y)}$[f]
PIPTPA	3.08	11,711	6.86	5.29	3.75	515 (75)	(0.274, 0.449)
PITTPA	2.95	10,844	7.42	5.77	4.14	495 (68)	(0.273, 0.419)

[a] Device configuration: ITO (120 nm)/F_4TCNQ (4 nm)/α-NPD (40 nm)/TPA (50 nm)/BCP (10 nm)/LiF (0.5 nm)/Al (150 nm).
[b] V_{onset}: turn-on voltage at a luminance of 1 cd m^{-2}.
[c] L_{max}: Maximum luminance at 15 V.
[d] η_c: Current, power and external quantum efficiencies measured at 100 cd m^{-2}.
[e] λ_{em}: Emission wavelength maximum. FWHM: full-width half maximum at 10 V.
[f] CIE color coordinates.

centered at 515 and 495 nm, respectively with full-width at half maxima (FWHM) of 75 and 68 nm. The CIE chromaticity coordinates of the derivatives as EL materials are determined using the EL spectra of the devices at 10 V. The chromaticity diagram is shown in Fig. 12A and the CIE coordinates are tabulated in Table 4. Furthermore, as shown in Fig. 12B, the EL spectra of both the devices showed the same profile without any effect on the shape and EL spectra peak under various driving voltages. Hence, both the devices exhibited excellent spectral stability over a wide range of operating voltages. The EL peaks (515 nm and 495 nm) show bathochromic shifts with respect to the thin film PL peaks (446 nm and 440 nm, Fig. 4). This bathochromic shift of EL peaks with respect to PL can be due to the interplay of charge carrier versus exciton dynamics and/or due to the result of excimer formation [36,37]. The insets in the Fig. 12 B show the digital image of the operational OLEDs.

4. Conclusion

In summary, we have successfully designed and synthesized star shaped electroluminescent phenanthroimidazole-based materials (donor–π-acceptor) by integrating the triphenylamine core (electron-donating moiety) to the phenanthroimidazole (electron-accepting moiety) with different linkers in N_1-position. The materials show good thermal stability as well as high glass transition temperatures. The electrochemical analysis reveals that both the materials have distinct oxidation and reduction behaviors. OLED device with PITTPA emitter

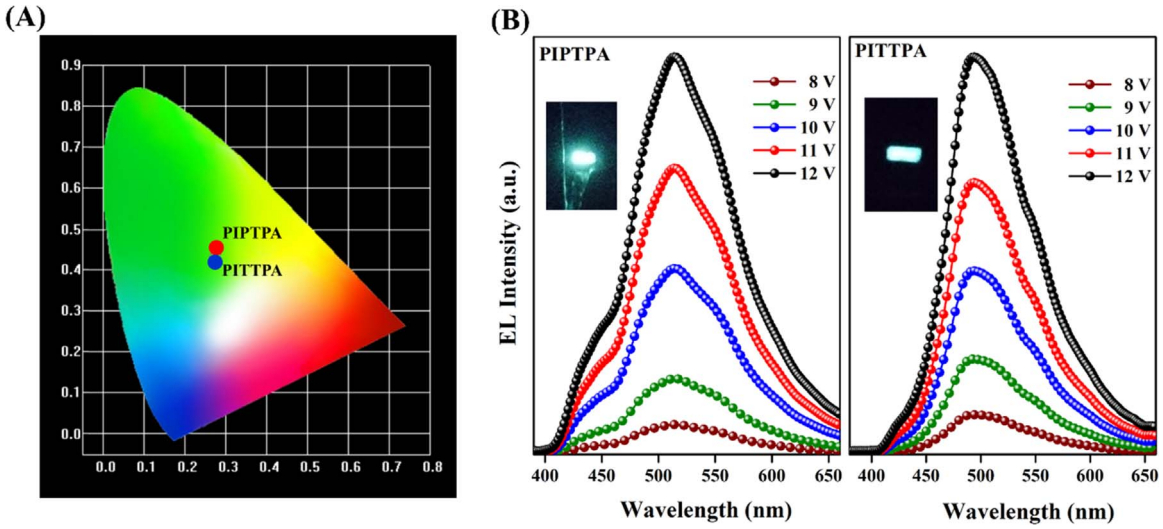

Fig. 12. (A) Chromaticity diagram and (B) EL spectra of the OLEDs at different applied voltages (insets show the image of the operational OLEDs).

exhibits high efficiencies (7.42 cd/A, 5.77 lm/W, and 4.14%) with low turn-on voltage of 2.95 V than that of PIPTPA (6.86 cd/A, 5.29 lm/W, 3.75%, turn-on voltage: 3.08 V). Both the materials show green emission with CIE coordinates of (0.274, 0.449) and (0.273, 0.419) for PIPTPA and PITTPA, respectively. These results demonstrate that these derivatives are promising candidates and could play an important role in the development of non-doped OLEDs.

Supplementary data

Supporting Information consist of NMR spectra (^{1}H and ^{13}C) and mass spectra of the materials. Solvatochromism, Lippert–Mataga equation study, atom coordinates and absolute energies (DFT).

Acknowledgements

T. J. and V. S. acknowledge INSPIRE, DST, India (FACULTY AWARD no.: IFA12-CH-48) for the financial support. The authors thank Dr. Kartick Tarafder, Department of Physics, National Institute of Technology, Surathkal, Mangalore, India, for the computational study.

Appendix A. Supplementary material

Supplementary data associated with this article can be found in the online version at http://dx.doi.org/10.1016/j.jlumin.2017.09.020.

References

[1] C.W. Tang, S.A. VanSlyke, Appl. Phys. Lett. 51 (1987) 913.
[2] J.H. Burroughes, D.C. Bradley, A.R. Brown, R.N. Marks, K. Mackay, R.H. Friend, P.L. Burns, A.B. Holmes, Nature 347 (1990) 539–541.
[3] M.A. Baldo, D.F. O'Brien, Y. You, A. Shoustikov, S. Sibley, M.E. Thompson, S.R. Forrest, Nature 395 (1998) 151–154.
[4] M. Zhu, C. Yang, Chem. Soc. Rev. 42 (2013) 4963–4976.
[5] P.I. Shih, Y.H. Tseng, F.I. Wu, A.K. Dixit, C.F. Shu, Adv. Funct. Mater. 16 (2006) 1582–1589.
[6] K. Okumoto, H. Kanno, Y. Hamaa, H. Takahashi, K. Shibata, Appl. Phys. Lett. 89 (2006) 063504.
[7] Y. Li, M.K. Fung, Z. Xie, S.T. Lee, L.S. Hung, J.J. Shi, Adv. Mater. 14 (2002) 1317–1321.
[8] M.A. Baldo, C. Adachi, S.R. Forrest, Phys. Rev. B 62 (2000) 10967–10977.
[9] N. Matsumoto, T. Miyazaki, M. Nishiyama, C. Adachi, J. Phys. Chem. C 113 (2009) 6261.
[10] Y.X. Yang, P. Cohn, A.L. Dyer, S.H. Eom, J.R. Reynolds, R.K. Castellano, J.G. Xue, Chem. Mater. 22 (2010) 3580.
[11] Y. Tao, C. Yang, J. Qin, Soc. Rev. 40 (2011) 2943–2970.
[12] M.H. Tsai, H.W. Lin, H.C. Su, T.H. Ke, C.C. Wu, F.C. Fang, Y.L. Liao, K.T. Wong, C.I. Wu, Adv. Mater. 18 (2006) 1216–1220.
[13] J. Li, D. Liu, Y. Li, C.S. Lee, H.L. Kwong, S. Lee, Chem. Mater. 17 (2005) 1208.
[14] J. Jin, W. Zhang, B. Wang, G. Mu, P. Xu, L. Wang, H. Huang, Chem. Mater. 26 (2014) 2388–2395.
[15] H. Inomata, K. Goushi, T. Masuko, T. Konno, T. Imai, H. Sasabe, J.J. Brown, C. Adachi, Chem. Mater. 16 (2004) 1285.
[16] Y. Sun, L. Duan, D. Zhang, J. Qiao, G. Dong, L. Wang, Y. Qiu, Adv. Funct. Mater. 21 (2011) 1881.
[17] K. Wang, S. Wang, J. Wei, Y. Miao, Y. Liu, Y. Wang, Org. Electron. 15 (2014) 3211–3220.
[18] W. Li, D. Liu, F. Shen, D. Ma, Z. Wang, T. Feng, Y. Xu, B. Yang, Y. Ma, Adv. Funct. Mater. 22 (2012) (2797–03).
[19] H. Huang, Y. Wang, B. Wang, S. Zhuang, B. Pan, X. Yang, L. Wang, C. Yang, J. Mater. Chem. C 1 (2013) (5899–08).
[20] D. Liu, M. Du, D. Chen, K. Ye, Z. Zhang, Y. Liu, Y. Wang, J. Mater. Chem. C 3 (2015) 4394.
[21] W. Qin, Z. Yang, Y. Jiang, J.W.Y. Lam, G. Liang, H.S. Kwok, B.Z. Tang, Chem. Mater. 27 (2015) (3892–01).
[22] S. Chen, Y. Wu, Y. Zhao, D. Fang, RSC Adv. 5 (2015) 72009.
[23] H. Huang, Y. Wang, S. Zhuang, X. Yang, L. Wang, C. Yang, J. Chen, D. Ma, J. Phys. Chem. C 116 (2012) 19458–19466.
[24] Y.X. Wang, Mk Leung, Macromolecules 44 (2011) 8771–8779.
[25] J. Jayabharathi, P. Ramanathan, V. Thanikachalam, C. Karunakaran, New J. Chem. 39 (2015) 3801–3812.
[26] S.A. VanSlyke, C.H. Chen, C.W. Tang, Appl. Phys. Lett. 69 (1996) 2160.
[27] R.J. Holmes, S.R. Forrest, Y.J. Tung, R.C. Kwong, J.J. Brown, S. Garon, M.E. Thompson, Appl. Phys. Lett. 82 (2003) 15.
[28] W.C. Chen, Y. Yuan, G.F. Wu, H.X. Wei, J. Ye, M. Chen, F. Lu, Q.X. Tong, F.L. Wong, C.S. Lee, Org. Electron. 17 (2015) 159–166.
[29] S. Kasturi, V. Sivakumar, RSC Adv. 6 (2016) 98652–98662.
[30] X. Ban, W. Jiang, K. Sun, X. Xie, L. Peng, H. Dong, Y. Sun, B. Huang, L. Duan, Y. Qiu, Appl. Mater. Interfaces 7 (2015) 7303–7314.
[31] H. Ulla, B. Garudachari, M.N. Satyanarayan, G. Umesh, A.M. Isloor, Opt. Mater. 36 (2014) 704–711.
[32] A. Filarowski, M. Kluba, K.C. Boczula, A. Koll, A. Kochel, L. Pandey, W.M.D. Borggraeve, M.V.D. Auweraer, J. Catalanc, N. Boens, Photochem. Photobiol. Sci. 9 (2010) (996-08).
[33] M.J. Frisch, et al., Gaussian 09, Revision D.01, Gaussian, Inc., Wallingford, CT, 2009.
[34] Y. Tao, Q. Wang, L. Ao, C. Zhong, J. Qin, C. Yang, D. Ma, J. Mater. Chem. 20 (2010) 1759–1765.
[35] D.M. Leeuw, M.M.J. Simenon, A.R. Brown, R.E.F. Einerhand, Synth. Met. 87 (1997) 53–59.
[36] J.M. Fernandes, M. Raveendra Kiran, H. Ulla, M.N. Satyanarayan, G. Umesh, Superlattices Microstruct. 76 (2014) 385–393.
[37] J.M. Fernandes, M.R. Kiran, H. Ulla, M.N. Satyanarayan, G. Umesh, Superlattices Microstruct. 83 (2015) 766–775.
[38] S. Chidirala, H. Ulla, A. Valaboju, M.R. Kiran, M.E. Mohanty, M.N. Satyanarayan, G. Umesh, K. Bhanuprakash, V.J. Rao, J. Org. Chem. 81 (2016) 603–614.
[39] H. Ulla, M. Raveendra Kiran, B. Garudachari, M.N. Satyanarayan, G. Umesh, A.M. Isloor, Opt. Mater. 37 (2014) 311–321.
[40] C.G. Zhen, Y.F. Dai, W.J. Zeng, Z. Ma, Z.K. Chen, J. Kieffer, Adv. Funct. Mater. 21 (2011) (699–07).